Seventh International Conference on Computational Fluid Dynamics (ICCFD7), Big Island, Hawaii, July 9-13, 2012

ICCFD7-3302

Viscoplastic Free-Surface Flows: The Herschel-Bulkley Case

C. Acary-Robert, E.D. Fernández-Nieto, G. Narbona-Reina and P. Vigneaux*

* Corresponding author: Paul.Vigneaux@math.cnrs.fr
Unité de Mathématiques Pures et Appliquées,
Ecole Normale Supérieure de Lyon. 46 allée d'Italie. 69364 Lyon Cedex 07, France.

Abstract: In this paper, we will describe consistent numerical methods for power-law viscoplastic free-surface flows. From the rheological viewpoint, associated models are of Herschel-Bulkley type, which is a generalization of the Bingham model. On the one hand, Bingham model is the simplest model when it comes to describe viscoplasticity. On the other hand, power-law model is a natural extension of a rate-of-shear dependant viscosity, as opposed to the canical case of the (often) constant viscosity used in the Navier-Stokes equations. After describing a shallow-water asymptotics of a 3D Navier-Stokes-Herschel-Bulkley model with free surface, we will end up with a model which has various mathematical difficulties. We will show how to handle optimization problems arising from the variational inequalities associated to the model, as well as their coupling with finite-volume discretization. Several numerical tests will be shown, including a comparison with an analytic solution, to confirm the well balanced property and the ability to cope with the various rheological regimes associated with the Herschel-Bulkley constitutive law.

Keywords: variational inequality, finite volume, well balanced, Herschel-Bulkley, viscous shallow water, avalanche.

1 Introduction

In this article, we are interested in the derivation of an integrated Herschel-Bulkley model for shallow flows. The goal is to simulate the evolution of thin sheet of *viscoplastic materials* on inclined planes and, in particular, to be able to compute the evolution from dynamic to stationary states. This raises the need for new numerical algorithms to solve consistently the resulting equations.

Viscoplastic materials are characterised by the existence of a yield stress: below a certain critical threshold in the imposed stress, there is no deformation and the material behaves like a rigid solid, but when that yield value is exceeded, the material flows like a fluid. Such flow behaviour can be encountered in many practical situations such as food pastes, cosmetics creams, heavy oils, mud and clays, lavas and avalanches. As a consequence, the theory of the fluid mechanics of such materials has applications in a wide variety of fields ranging from food industry to geophysical fluid dynamics.

Among numerous models used to describe the rheology of viscoplastic materials, Bingham (linear model with plasticity, [4]) and Herschel-Bulkley (power law model with plasticity, [11]) models are probably the most iconic. The Herschel-Bulkley model is expressed as :

$$\begin{aligned} \sigma' &= \left(2^{\wp} K |D(u)|^{\wp-1} + \tau_y \frac{1}{|D(u)|}\right) D(u), && \text{if } |D(u)| \neq 0, \\ |\sigma'| &\leq \tau_y, && \text{if } |D(u)| = 0, \end{aligned} \tag{1}$$

where K is the consistency, τ_y is the yield stress and $|D(u)|$ is the second invariant of the rate of strain (we will give complete definitions and notations in the following section). This model can be seen as a generalization of the Bingham model which is retrieved from (1) by taking $\wp = 1$. On the one hand, Bingham model is the simplest model when it comes to describe plasticity. On the other hand, if we take $\tau_y = 0$ and $\wp < 1$, we end up with the classical power-law (shear-thinning) model. Evidently, if $\tau_y = 0$ and $\wp = 1$, (1) leads to the classic Navier-Stokes equations.

Apart from the difficulty associated to the constitutive relation, there is another source of complication associated to the flows we are considering here: we have to deal with free surfaces. Even if it is now possible to compute such 3D flows by solving the full equations, it must be noted that the global computational time is still very expensive, especially if one wants to reach long physical times to study the stopping dynamics of the material (such times can be rather long depending on the value of τ_y). The classical idea is thus to rely on reduced models, in such a way important physical features are retained as much as possible, but computational difficulties are significantly smoothed out. In the context of non-Newtonian fluids, there are essentially two families of approaches to deal with this issue: lubrication theory and shallow water models. On the one hand, in lubrication models, fluid velocity and pressure are determined by the local fluid height and its derivatives. Originally, these methods were derived for gentle slopes and thin flows. Nevertheless, they can be extended to the case of steep slopes, as it was pointed out by Balmforth et al. in [3]. On the other hand, for thicker flows, shallow water approaches consist in deriving governing equations by averaging the local mass and momentum equations across the stream depth. In [5], a shallow water model is derived by considering a constant profile for the velocity along the vertical and using a variational formulation of the Navier-Stokes equations for Bingham fluids, by choosing convenient test functions.

In this paper, we extend our previous work [5], dedicated to Bingham model, by considering instead the model (1). This allows us to tackle practical situations, such as the one presented in [2]. More precisely, starting from a 3D incompressible fluid modelled by the Navier-Stokes equations, together with the Herschel-Bulkley constitutive law (1), and with a free surface, we introduce its formulation as a variational inequality and derive a shallow water asymptotic of this system. To solve numerically the obtained model, we need to treat the optimization problem coming from the plastic behavior of the material: this is done with an augmented Lagrangian approach inspired by the seminal work of Glowinski and coworkers (see [7] for a recent review). In the context of shallow water problems, we adopt a finite volume approach to discretize the equations. A careful treatment must be made to design a *well-balanced* scheme when coupling the finite volume scheme and the augmented Lagrangian method. This idea was first introduced in [5], in the context of a *linear* viscoplastic law, and is extended here to the case of a *power* viscoplastic law such as (1).
Let us note that the present length-constrained conference paper have an extended companion paper, in a forthcoming issue of the *Journal of Scientific Computing*, [1], to which the reader is kindly referred for the complete details about this work.

The structure of the paper is as follows. In section 2, we present the derivation of the model which will be considered and describe its rheological properties in section 3. We then propose, in section 4, a consistent scheme to solve this model, in the sense that it allows to compute the stationnary states that can be encountered in practical situations. The properties of this scheme are thus confirmed numerically in section 5.

2 Derivation of the Herschel-Bulkley shallow water model

Let us start from the governing equations for a Herschel-Bulkley fluid confined to a domain $\mathcal{D}(t) \subset \mathbb{R}^3$ with a smooth boundary $\partial\mathcal{D}(t)$.
Since we deal with an incompressible fluid, we have

$$\text{div } \boldsymbol{u} = 0 \quad \text{ in } \mathcal{D}(t), \tag{2}$$

where $\boldsymbol{u}$ is the Eulerian velocity field. We consider the time interval $(0, T)$ with $T > 0$ to solve the evolution problem.

In the following, the space and time coordinates as well as all mechanical fields are non dimensional, so we introduce some notations for the characteristic variables: ρ_c, V_c, L_c, T_c, f_c, τ_c and p_c corresponding respectively to density, velocity, length, time, body force, yield stress and pressure.
The conservation of mass is given by

$$\mathrm{St}\frac{\partial \rho}{\partial t} + \boldsymbol{u}\cdot\nabla\rho = 0 \quad \text{ in } \mathcal{D}(t) \tag{3}$$

where $\rho = \rho(t,x) \geq \underline{\rho} > 0$ is the mass density distribution and $\mathrm{St} = L_c/(V_c T_c)$ is the Strouhal number.

For incompressible fluids, the stress tensor $\boldsymbol{\sigma}$ is usually decomposed into an isotropic part $-p\mathbf{I}$ where $p = -\operatorname{trace}(\boldsymbol{\sigma})/3$ represents the pressure field and a remainder called the deviatoric part of the stress tensor $\boldsymbol{\sigma}' = \boldsymbol{\sigma} + p\mathbf{I}$. Thus, momentum balance law in Eulerian coordinates reads

$$\rho\Big(\mathrm{St}\frac{\partial \boldsymbol{u}}{\partial t} + (\boldsymbol{u}\cdot\nabla)\boldsymbol{u}\Big) - \mathbf{div}\,\boldsymbol{\sigma}' + \frac{1}{\mathrm{Fr}^2}\nabla p = \frac{1}{\mathrm{Fr}^2}\rho\boldsymbol{f} \quad \text{ in } \mathcal{D}(t), \tag{4}$$

where $\boldsymbol{f}$ denotes the body forces. The Froude number is $\mathrm{Fr}^2 = \rho_c V_c^2/p_c$ where the characteristic pressure is chosen as $p_c = \rho_c f_c L_c$.

With the definition of the deviatoric stress, we specify the rheology of the fluid and we get a closed problem together with conservation of mass and momentum (3), (4). We write the constitutive law for a Herschel-Bulkley fluid:

$$\boldsymbol{\sigma}' = \frac{2}{\mathrm{Re}}\eta_1\frac{\boldsymbol{D}(\boldsymbol{u})}{|\boldsymbol{D}(\boldsymbol{u})|^{1-\wp}} + \tau_y\mathrm{B}\frac{\boldsymbol{D}(\boldsymbol{u})}{|\boldsymbol{D}(\boldsymbol{u})|} \qquad \text{if } |\boldsymbol{D}(\boldsymbol{u})| \neq 0, \tag{5}$$

$$|\boldsymbol{\sigma}'| \leq \tau_y\mathrm{B} \qquad \text{if } |\boldsymbol{D}(\boldsymbol{u})| = 0, \tag{6}$$

where $\boldsymbol{D}(\boldsymbol{u}) = (\boldsymbol{\nabla u} + \boldsymbol{\nabla}^T\boldsymbol{u})/2$ is the rate of strain tensor, $|\boldsymbol{D}(\boldsymbol{u})| = (\sum_{i,j=1}^3[(\boldsymbol{\nabla u} + \boldsymbol{\nabla}^T\boldsymbol{u})/2]_{ij}^2)^{1/2}$ and $0 < \wp < 1$ is the power associated to the Herschel-Bulkley law. For this range of values the effective viscosity decreases with the amount of deformation, leading to the so-called shear-thinning effect. The coefficient $\eta_1 \geq \underline{\eta} > 0$ is defined as a function of $\wp$ and the consistency K through,

$$\eta_1 = 2^{\wp-1}K. \tag{7}$$

When considering a density-dependent model, the coefficient η_1 depends on the density ρ through a constitutive function, *i.e.*

$$\eta_1 = \eta_1(\rho). \tag{8}$$

The Reynolds and the Bingham numbers, are respectively defined as

$$\mathrm{Re} = \frac{\rho_c V_c L_c}{K\left(\frac{V_c}{L_c}\right)^{\wp-1}}, \quad \mathrm{Bi} = \frac{\tau_c L_c^{\wp}}{K V_c^{\wp}},$$

and we also define the quotient $\mathrm{B} = \mathrm{Bi}/\mathrm{Re}$.

For boundary conditions, we assume that $\partial\mathcal{D}(t)$ is split in two disjoint parts: $\partial\mathcal{D}(t) = \Gamma_b(t)\cup\Gamma_s(t)$ where $\Gamma_b(t)$ is the part of the fluid which is on the solid bottom, and $\Gamma_s(t)$ is the free surface region.
We will denote as $\boldsymbol{n}$ the outward unit normal on $\partial\mathcal{D}(t)$ and we adopt the following notation for the tangential and normal decomposition of any velocity field $\boldsymbol{u}$ and any density of surface forces $\boldsymbol{\sigma n}$,

$$\boldsymbol{u} = u_n\boldsymbol{n} + \boldsymbol{u}_t, \ \text{ with } \ u_n = \boldsymbol{u}\cdot\boldsymbol{n}, \qquad \boldsymbol{\sigma n} = \sigma_n\boldsymbol{n} + \boldsymbol{\sigma}_t \ \text{ with } \ \sigma_n = \boldsymbol{\sigma n}\cdot\boldsymbol{n}.$$

On $\Gamma_b(t)$, we consider a Navier condition with a friction coefficient α and a no-penetration condition

$$\boldsymbol{\sigma}_t = -\alpha\boldsymbol{u}_t, \qquad \boldsymbol{u}\cdot\boldsymbol{n} = 0 \quad \text{on} \quad \Gamma_b(t). \tag{9}$$

As usual for a free surface, we assume a no-stress condition

$$\boldsymbol{\sigma}\boldsymbol{n} = 0 \qquad \text{on} \quad \Gamma_s(t), \tag{10}$$

and the advection of the fluid by the flow:

$$\mathrm{St}\frac{\partial 1_{\mathcal{D}(t)}}{\partial t} + \boldsymbol{u}\cdot\nabla 1_{\mathcal{D}(t)} = 0, \tag{11}$$

where $1_{\mathcal{D}(t)}$ is the characteristic function of the domain $\mathcal{D}(t)$.

Finally, we denote initial conditions as:

$$\boldsymbol{u}|_{t=0} = \boldsymbol{u}^0, \quad \rho|_{t=0} = \rho^0. \tag{12}$$

To tackle this problem, we opt for a variational formulation, originally presented by Duvaut-Lions in [8]. We formulate the problem in terms of velocity and pressure, by considering the space:

$$\mathcal{W}(t) = \big\{\boldsymbol{\Phi} \in W^{1,1+\wp}(\mathcal{D}(t))^3 \ / \quad \boldsymbol{\Phi}\cdot\boldsymbol{n} = 0 \ \text{ on } \ \Gamma_b(t)\big\}.$$

It reads:

$$\begin{cases} \forall t\in(0,T), \quad \boldsymbol{u}(t,\cdot)\in\mathcal{W}(t),\ p(t,\cdot)\in L^{1+\wp}(\mathcal{D}(t)), \quad \forall\boldsymbol{\Phi}\in\mathcal{W}(t),\ \forall q\in L^{1+\wp}(\mathcal{D}(t)) \\ \displaystyle\int_{\mathcal{D}(t)}\rho\Big(\mathrm{St}\frac{\partial\boldsymbol{u}}{\partial t} + (\boldsymbol{u}\cdot\nabla)\boldsymbol{u}\Big)\cdot(\boldsymbol{\Phi}-\boldsymbol{u}) - \frac{1}{\mathrm{Fr}^2}\int_{\mathcal{D}(t)} p(\operatorname{div}\boldsymbol{\Phi} - \operatorname{div}\boldsymbol{u}) + \\ \displaystyle\frac{1}{\mathrm{Re}}\int_{\mathcal{D}(t)} 2\eta_1(\rho)\frac{\boldsymbol{D}(\boldsymbol{u})}{|\boldsymbol{D}(\boldsymbol{u})|^{1-\wp}} : (\boldsymbol{D}(\boldsymbol{\Phi}) - \boldsymbol{D}(\boldsymbol{u})) + \tau_y\mathrm{B}\int_{\mathcal{D}(t)}(|\boldsymbol{D}(\boldsymbol{\Phi})| - |\boldsymbol{D}(\boldsymbol{u})|) + \\ \displaystyle\int_{\Gamma_b(t)}\alpha\boldsymbol{u}_t\cdot(\boldsymbol{\Phi}_t - \boldsymbol{u}_t) \geq \frac{1}{\mathrm{Fr}^2}\int_{\mathcal{D}(t)}\rho\boldsymbol{f}\cdot(\boldsymbol{\Phi}-\boldsymbol{u}), \\ \displaystyle\int_{\mathcal{D}(t)} q\operatorname{div}\boldsymbol{u} = 0. \end{cases} \tag{13}$$

We can then derive a shallow water asymptotics of this model. For sake of brevity, we refer to the companion paper [1] for the 2D version and present the 1D viscous Shallow Water formulation for a Herschel-Bulkley type fluid. If H is the height of the fluid, $\boldsymbol{V}_0$ the height-averaged velocity and $\boldsymbol{\Psi}$ a test function, we have $\forall(x,t)\in[0,L]\times[0,T]$, $H = H(x,t)$, $\overline{\rho_0} = \overline{\rho_0}(x,t)$, $\boldsymbol{V}_0 = \boldsymbol{V}_0(x,t)$,

$$\mathrm{St}\frac{\partial H}{\partial t} + \frac{\partial(H\boldsymbol{V}_0)}{\partial x} = 0, \tag{14}$$

$$\mathrm{St}\frac{\partial(\overline{\rho_0}H)}{\partial t} + \frac{\partial(H\overline{\rho_0}\boldsymbol{V}_0)}{\partial_x} = 0, \tag{15}$$

$$\begin{aligned} &\forall\boldsymbol{\Psi}, \quad \int_0^L H\overline{\rho_0}\Big(\mathrm{St}\partial_t\boldsymbol{V}_0(\boldsymbol{\Psi}-\boldsymbol{V}_0) + \frac{1}{2}\partial_x(\boldsymbol{V}_0^2)(\boldsymbol{\Psi}-\boldsymbol{V}_0)\Big)dx \\ &+ \int_0^L\tilde{\beta}\boldsymbol{V}_0(\boldsymbol{\Psi}-\boldsymbol{V}_0)dx + \int_0^L\frac{2^{\frac{3+\wp}{2}}}{\mathrm{Re}}H\frac{\overline{\eta_1(\rho_0)}}{|\partial_x\boldsymbol{V}_0|^{1-\wp}}\partial_x(\boldsymbol{V}_0)\partial_x(\boldsymbol{\Psi}-\boldsymbol{V}_0)dx \\ &+ \int_0^L\tau_y\mathrm{B}H\sqrt{2}\Big(|\partial_x\boldsymbol{\Psi}| - |\partial_x\boldsymbol{V}_0|\Big)dx \\ &\geq \frac{1}{\mathrm{Fr}^2}\int_0^L H\overline{\rho_0}\tilde{f}_x(\boldsymbol{\Psi}-\boldsymbol{V}_0) - \frac{1}{\mathrm{Fr}^2}\int_0^L\frac{f_z}{2}H^2\overline{\rho_0}(\partial_x\boldsymbol{\Psi} - \partial_x\boldsymbol{V}_0)dx. \end{aligned} \tag{16}$$

This model contains several difficulties both from the theoretical and numerical viewpoints; among them are viscoplasticity effects. In this paper, we focus on the design of numerical algorithms which handle the

mathematical features of viscoplasticity effects associated to the Herschel-Bulkley law. By the way, in the following, we will consider that the density $\rho_0 = \rho$ is constant in time and in space. This implies that (14)-(15) reduce to (14). Moreover, for the sake of readability, we denote $\boldsymbol{V}_0$ by $\boldsymbol{V}$. Finally, we will take the gravity for the external forces :

$$f_x = -g\sin\theta, \quad f_z = -g\cos\theta.$$

Then, going back to *dimensional variables*, the model under consideration will be:

$$\frac{\partial H}{\partial t} + \frac{\partial (H\boldsymbol{V})}{\partial x} = 0, \tag{17}$$

$$\begin{aligned}
&\forall \boldsymbol{\Psi}, \quad \int_0^L H\Big(\partial_t \boldsymbol{V}(\boldsymbol{\Psi}-\boldsymbol{V}) + \frac{1}{2}\partial_x(\boldsymbol{V}^2)(\boldsymbol{\Psi}-\boldsymbol{V})\Big)dx \\
&+ \int_0^L \tilde{\alpha}\boldsymbol{V}(\boldsymbol{\Psi}-\boldsymbol{V})dx + \int_0^L 2^{\frac{3+\wp}{2}} H \frac{\nu_1}{|\partial_x \boldsymbol{V}|^{1-\wp}}\partial_x(\boldsymbol{V})\partial_x(\boldsymbol{\Psi}-\boldsymbol{V})dx \\
&+ \int_0^L \tau_y\sqrt{2}H\Big(|\partial_x\boldsymbol{\Psi}| - |\partial_x\boldsymbol{V}|\Big)dx \\
&\geq -g\sin\theta\int_0^L H(\boldsymbol{\Psi}-\boldsymbol{V}) + g\frac{\cos\theta}{2}\int_0^L H^2(\partial_x\boldsymbol{\Psi} - \partial_x\boldsymbol{V})dx,
\end{aligned} \tag{18}$$

where $\nu_1 = \eta_1/\rho$ is the viscosity coefficient, τ_y is the yield stress, g is the constant of gravity and $\tilde{\alpha} = \beta/\rho$ is the friction coefficient between the material and the bottom.

3 Rheological properties of the model

We detail now the constitutive law associated to the rheology of the integrated model (18). We are here in 1D; if we denote the shear stress by σ and the rate of shear by $\dot{\gamma}$, the constitutive law is:

$$\sigma(\dot{\gamma}) = 2^{\frac{3+\wp}{2}}\ \nu_1\ \frac{\dot{\gamma}}{|\dot{\gamma}|^{1-\wp}} + \tau_y\sqrt{2}\frac{\dot{\gamma}}{|\dot{\gamma}|}, \qquad \text{if } \dot{\gamma}\neq 0, \tag{19}$$

$$|\sigma(\dot{\gamma})| \ \leq\ \tau_y\sqrt{2}, \qquad \text{if } \dot{\gamma} = 0. \tag{20}$$

Note that in this 1D case, we have $\dot{\gamma}$ which is given by $\partial_x V$. The idea is to compare the associated curves for different values of the Herschel-Bulkley parameter $\wp$. To have a graphical view of such variety, let us suppose that the viscosity $\nu_1 = 1$, the yield stress $\tau_y = 6/\sqrt{2}$ and that we consider three types of fluid with respect to $\wp$, namely $\wp = 1$ (which is actually the special case of a Bingham fluid), $\wp = 0.7$ and $\wp = 0.4$. The curves are shown on Figure 1.

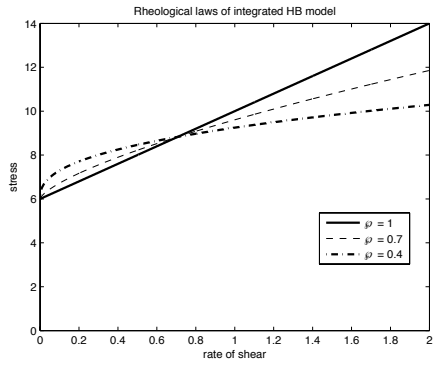

Figure 1: Various Herschel-Bulkley constitutive models for $\wp = 1, 0.7, 0.4$.

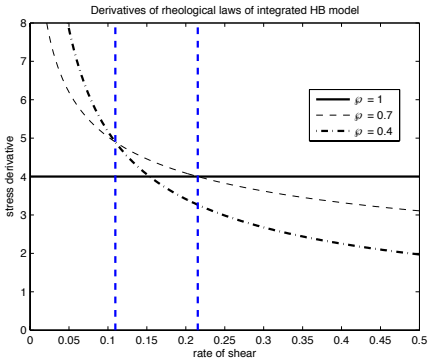

Figure 2: Derivatives of various Herschel-Bulkley constitutive models for $\wp = 1, 0.7, 0.4$. The vertical dashed lines separate three zones. The one on the left (**Zone 1**, $\dot{\gamma} \leq 0.11$) is used for the third test in section 5, whereas the one on the right (**Zone 3**, $\dot{\gamma} \geq 0.22$) is used for the second test in section 5.

The interesting point is to look at the derivatives of these three curves in order to have an idea of the viscosity (in the generalized sense). This will show which fluid is the more likely to flow faster for a given rate of shear. These three derivatives are shown on Figure 2. On this Figure we put two vertical (dashed) lines to show three zones:

- on the left (denoted as **Zone 1**), a zone where the Bingham fluid is the *less "viscous"* of the three fluids, followed in this order by the Herschel-Bulkley fluids $\wp = 0.7$ and $\wp = 0.4$;
- on the right (denoted as **Zone 3**), a zone completely opposed to the previous one, where the Bingham fluid is the *more "viscous"* of the three fluids, followed in this order by the Herschel-Bulkley fluids $\wp = 0.7$ and $\wp = 0.4$;
- an intermediate zone (denoted as **Zone 2**) where there is no clear order in terms of the viscosity of the three fluids.

In the numerical tests we perform in this paper (see second and third tests of section 5), we inspired ourselves by Figure 2 by performing a test where the Bingham fluid is the most viscous: to do so, we need to design a test with high rates of shear, in the sense that a significant part of the fluid experiences rate of shear $\dot{\gamma} \geq x_2 \sim 0.22$ (with the choice of parameters given above), in such a way it corresponds to Zone 3.

On the other hand, the Zone 1 ($\dot{\gamma} \leq x_1 \sim 0.1$) is naturally explored for all tests where we check the stationary states where V and $\partial_x V$ are zero, or very close to zero.

4 Blending well-balanced schemes and augmented Lagrangian

We consider a backward Euler time discretization for equations (17)-(18)

$$\frac{H^{n+1} - H^n}{\Delta t} + \frac{\partial (H^n \boldsymbol{V}^n)}{\partial x} = 0, \tag{21}$$

$$
\begin{aligned}
&\forall \boldsymbol{\Psi}, \quad \int_0^L H^n \Big(\frac{\boldsymbol{V}^{n+1}-\boldsymbol{V}^n}{\Delta t}(\boldsymbol{\Psi}-\boldsymbol{V}^{n+1}) + \frac{1}{2}\partial_x(\boldsymbol{V}^n)^2(\boldsymbol{\Psi}-\boldsymbol{V}^{n+1}) \Big) dx \\
&+ \int_0^L \tilde{\alpha}\boldsymbol{V}^{n+1}(\boldsymbol{\Psi}-\boldsymbol{V}^{n+1})dx + \int_0^L 2^{\frac{3+\wp}{2}} H^n \frac{\nu_1}{|\partial_x \boldsymbol{V}^{n+1}|^{1-\wp}} \partial_x(\boldsymbol{V}^{n+1})\partial_x(\boldsymbol{\Psi}-\boldsymbol{V}^{n+1})dx \\
&+ \int_0^L \tau_y\sqrt{2} H^n \Big(|\partial_x \boldsymbol{\Psi}| - |\partial_x \boldsymbol{V}^{n+1}| \Big) dx \\
&\geq -g\sin\theta \int_0^L H^n(\boldsymbol{\Psi}-\boldsymbol{V}^{n+1}) + g\frac{\cos\theta}{2}\int_0^L (H^n)^2(\partial_x\boldsymbol{\Psi}-\partial_x\boldsymbol{V}^{n+1})dx,
\end{aligned}
\tag{22}
$$

where Δt is the time step and superscripts with n refer to time iteration at $t^n = n\Delta t$.

Directly inspired by book [9] on augmented Lagrangian methods, we can rewrite (22) as an optimization problem on $\boldsymbol{V}^{n+1}$:

$$
\mathcal{J}^n(\boldsymbol{V}^{n+1}) \quad = \quad \min_{\boldsymbol{V}\in\mathcal{V}} \mathcal{J}^n(\boldsymbol{V}). \tag{23}
$$

For sake of brevity, we do not describe $\mathcal{J}^n$ but we give directly the resulting algorithm induced by the augmented Lagrangian method (see [1] for details).

Augmented Lagrangian algorithm

- **Initialization**: suppose that $\boldsymbol{V}^n$, H^n and μ^n are known. For $k=0$, we set $\boldsymbol{V}^k = \boldsymbol{V}^n$ and $\mu^k = \mu^n$.
- **Iterate**:
  - Find $q^{k+1} \in \mathcal{H}$ solution of

$$
\left(2^{\frac{\wp+3}{2}} \nu_1 |q^{k+1}|^{\wp-1} + r \right) q^{k+1} = (\mu^k + r\partial_x(\boldsymbol{V}^k)) \left(1 - \frac{\tau_y\sqrt{2}}{|\mu^k + r\partial_x \boldsymbol{V}^k|} \right)_+ . \tag{24}
$$

    The subscript "+" in the last term stands for the positive part ($\lambda_+ := \max(0,\lambda)$). This is a non-linear problem which is solved numerically with a fixed point-like method.
  - Find $\boldsymbol{V}^{k+1} \in \mathcal{V}$ solution of

$$
\begin{aligned}
H^n \frac{\boldsymbol{V}^{k+1}-\boldsymbol{V}^n}{\Delta t} + H^n\partial_x \left(\frac{(\boldsymbol{V}^n)^2}{2} + g\cos\theta H^n \right) - r\partial_x(H^n(\partial_x\boldsymbol{V}^{k+1} - q^{k+1})) \\
= -\tilde{\alpha}\boldsymbol{V}^{k+1} - gH^n\sin\theta + \partial_x(H^n\mu^k).
\end{aligned}
\tag{25}
$$

  - Update the Lagrange multiplier via

$$
\mu^{k+1} = \mu^k + r(\partial_x \boldsymbol{V}^{k+1} - q^{k+1}); \tag{26}
$$

  - Check convergence (see below) and update: $\boldsymbol{V}^k = \boldsymbol{V}^{k+1}$, $\mu^k = \mu^{k+1}$, $k = k+1$ and go to the next iteration ...
- ... **until** convergence is reached:

$$
\frac{\|\mu^{k+1} - \mu^k\|}{\|\mu^k\|} \leq tol. \tag{27}
$$

At convergence, we get the value of $\boldsymbol{V}^{n+1}$ by setting $\boldsymbol{V}^{n+1} = \boldsymbol{V}^{k+1}$ (in the numerical tests presented in this paper, we set $tol = 10^{-5}$). It is shown in [7, 9] that this algorithm converges to the saddle point of the augmented Lagrangian functional associated to (23).

To complete the discretization, it remains to describe the treatment of spatial derivatives, which will be done with a finite volume approach as mentioned previously. To do so, it is worth realizing that the underlying global problem coupling (21) and (22) involves the following system (using a cosmetic change of notation which will be useful in the presentation: H^{n+1} is denoted as H^{k+1}; again, note that H^{k+1} is not involved in the augmented Lagrangian algorithm and, so, does not change in this loop):

$$(P)^{n,k} \left\{ \begin{array}{l} \dfrac{H^{k+1}-H^n}{\Delta t} + \partial_x(H^n \boldsymbol{V}^n) = 0, \\ \\ H^n \dfrac{\boldsymbol{V}^{k+1}-\boldsymbol{V}^n}{\Delta t} + H^n \partial_x \left(\dfrac{(\boldsymbol{V}^n)^2}{2} + g\cos\theta H^n \right) - r\partial_x(H^n(\partial_x \boldsymbol{V}^{k+1} - q^{k+1})) \\ \qquad\qquad = -\tilde{\alpha}\boldsymbol{V}^{k+1} - gH^n \sin\theta + \partial_x(H^n \mu^k). \end{array} \right. \tag{28}$$

This problem can be seen as a semi-discretization in time of a parabolic system, which for $r = 0$ degenerates into a hyperbolic system with source terms. Although in terms of time discretization and augmented Lagrangian algorithm the problem is decoupled, we must consider the coupling between mass and momentum equations, in order to obtain a well-balanced solver. It is induced by the source terms involving topography and the Lagrange multiplier. This is well documented for shallow water type systems with source term defined by the topography. In our case, the extra difficulty is to treat the source term defined in terms of the Lagrange multiplier. The good news being that this coupling only needs to be done with all the quantities obtained at the convergence of the augmented Lagrangian algorithm.
The spatial discretization is thus obtained by using a the well-balanced approach described in [6], on $(P)^{n,k}$ (see [1] for details).

Finally, we describe the *well-balanced* property of the numerical scheme. By substituting $\boldsymbol{V} = 0$ in (18), we can characterize two types of stationary solutions. The first one corresponds to the case of an horizontal free surface (in the global frame of reference), *i.e.* a stationary solution with a constant free surface:

$$\forall x \in [0, L], \quad b(x) + H(x)\cos\theta = cst,$$

where $b(x) = x \sin\theta$. The second type of stationary solution is a constant height over an inclined slope. We can see that if

$$\forall x \in [0, L], \quad \left(x - \frac{L}{2}\right) \sin\theta \leq \frac{\tau_y \sqrt{2}}{g}, \tag{29}$$

then $H \equiv cst$ is a stationary solution of the system. We can show:

Proposition. Let $(H = H(x); \boldsymbol{V} \equiv 0)$ be a stationary solution of (18), and assume that the proposed numerical scheme uses the following initialization for μ:

$$\forall i, \quad \mu_{i+1/2} = \left(H(x_{i+1/2}) - H\Big(\frac{L}{2}\Big) \right) \cos\theta \; + \; \left(x_{i+1/2} - \frac{L}{2} \right) \sin\theta,$$

then, this scheme exactly preserves both stationary solutions: (i) horizontal free surface and (ii) constant height, verifying (29), over an inclined plane.

5 Numerical results

5.1 An analytical test

In this section, we consider a simplified case associated to the standard "duct flow". This degenerate model contains all difficulties associated to the numerical approximation of the Herschel-Bulkley model (optimization problem to compute $\boldsymbol{V}$ *and* non-linear root finding to compute q, as presented previously). Namely, for

this simpler case, the model (18) degenerates to:

$$\begin{aligned}\forall \boldsymbol{\Psi},\quad & \int_0^L \Big(\partial_t \boldsymbol{V}(\boldsymbol{\Psi}-\boldsymbol{V}) + 2^{\frac{3+\wp}{2}}\frac{\nu_1}{|\partial_x \boldsymbol{V}|^{1-\wp}}\partial_x(\boldsymbol{V})\partial_x(\boldsymbol{\Psi}-\boldsymbol{V})\Big)dx \\ & + \int_0^L \sqrt{2}\tau_y\Big(|\partial_x(\boldsymbol{\Psi})| - |\partial_x(\boldsymbol{V})|\Big)dx \geq \int_0^L f(\boldsymbol{\Psi}-\boldsymbol{V})dx\end{aligned} \tag{30}$$

where f is a constant force (if ones thinks back on the Poiseuille flow in a duct, f is the pressure gradient in the direction of the flow). In the duct, there is no equation associated to H, which is stationary and constant, $H = 1$; furthermore, we put $\tilde{\alpha} = 0$ (no friction) and we drop the non-linear term $\partial_x(\boldsymbol{V}^n)^2$ since we suppose that we are in a Stokes' regime.

In the model (30), the time derivative acts as a *relaxation* term in the sense that *(i)* there exists a stationary asymptotic solution u (when $t \to +\infty$) and that *(ii)* an initial data $\boldsymbol{V}$, different from this asymptotic solution, will converge in time to u. The interest of this test is that u is a non-trivial stationary solution: $u \not\equiv 0$.

This analytical stationary solution is (see [10]):

$$u(\xi) = \frac{\wp\, f^{1/\wp}}{\left(2^{\frac{3+\wp}{2}}\,\nu_1\right)^{1/\wp}(1+\wp)} \begin{cases} \left(\frac{L}{2}-\xi_o\right)^{\frac{1}{\wp}+1} & \text{if } 0 \leq \xi \leq \xi_o, \\ \left(\frac{L}{2}-\xi_o\right)^{\frac{1}{\wp}+1} - (\xi-\xi_o)^{\frac{1}{\wp}+1} & \text{if } \xi_o < \xi \leq \frac{L}{2}. \end{cases} \tag{31}$$

where $\xi = |x - \frac{L}{2}|$, $\xi_o = \dfrac{\sqrt{2}\tau_y}{f}$ and the domain is defined for $x \in [0, L]$.

In the following, we thus study the evolution of $\boldsymbol{V}(t)$ from the initial data: $\forall x \in [0, L], \boldsymbol{V}(t = 0, x) = 0$. Dirichlet boundary conditions are imposed:

$$\forall t \geq 0, \quad \boldsymbol{V}(t, 0) = 0, \quad \boldsymbol{V}(t, L) = 0.$$

The idea is to check the ability of the numerical method to converge to the stationary solution (31).

We compute the evolution of the solution with the proposed numerical scheme and we consider that we have a numerical stationary solution when the relative error between two iterations in time is smaller than 10^{-8}, that is

$$\frac{\|\boldsymbol{V}^{n+1} - \boldsymbol{V}^n\|_1}{\|\boldsymbol{V}^{n+1}\|_1} < 10^{-8}.$$

We set a domain of length $L = 1$, discretized with 100 points. Moreover, $\nu_1 = 0.2$ and $\tau_y = 4/\sqrt{2}$. We show the results for $\wp = 0.75$, where the force $f = 25$. Similar results are obtained for values of $\wp = 1$, 0.50 and 0.25 (see [1]).

Table 1: Test 1. Errors and order of convergence for $\wp = 0.75$

Cells	L^1 Error	Order	L^∞ Error	Order
25	$7.367E^{-02}$	-	$9.488E^{-02}$	-
50	$1.861E^{-02}$	1.984	$2.338E^{-02}$	2.020
100	$4.759E^{-03}$	1.967	$5.988E^{-03}$	1.965
200	$1.267E^{-03}$	1.909	$1.599E^{-03}$	1.904

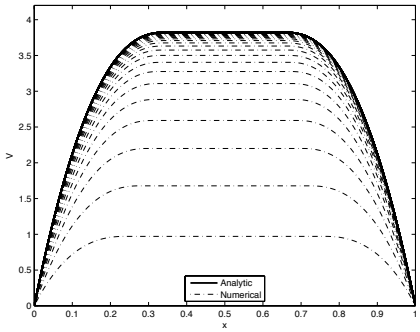

Figure 3: Test 1: Evolution of the computed velocity (dashed lines) to the analytical stationary solution (continuous line). $\wp = 0.75$. $\overline{\Delta t} = 0.1$, is the time separating each numerical curves.

In Figure 3, we present the convergence from the initial solution $\boldsymbol{V} \equiv 0$ to the stationary solution. In Table 1, the absolute errors between the numerical asymptotic solution and the analytical one are presented in norm L^1 and L^∞, as well as the associated order of the method. We observe that the method converges to the analytical stationary solution and that the convergence under mesh refinement is of second order in space.

5.2 A case at high rate of shear

In this section, we want to present the results of the method applied to a case where the rate of shear is high, in the sense that it is a regime where the Bingham fluid is the more "viscous" (compared to the Herschel-Bulkley fluid). This is a feature induced by the rheological richness of Herschel-Bulkley model, as shown in section 3.

Being concerned with high shear rate, the following test case is in opposition with the one in the next section where we will focus on the ability of the method to handle stationary states (which is linked to the well-balanced property of the method designed in this paper).

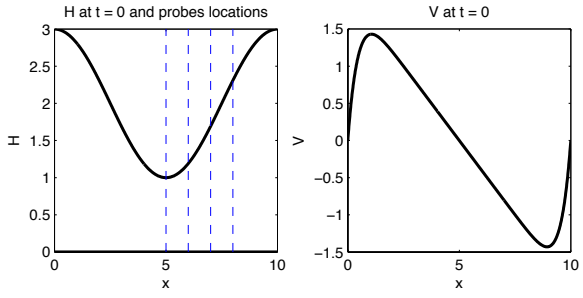

Figure 4: Initial conditions for the test with high rate of shear. The four dashed vertical lines indicate the probes' locations (denoted as Probe 1, 2, 3 and 4, from left to right respectively).

The test case is as follows. Physical parameters are those given in section 3. We consider an initial sinusoidal free surface over an horizontal slope ($\theta = 0$) as shown in Figure 4. We put a non zero initial velocity (see also Figure 4), which will act together with the gravity $g = 9.81$ to move the free surface.

Namely (the domain is $[0; L]$ with $L = 10$ and we use a discretization grid in space with 1000 points; furthermore, there is no friction):

$$H(t = 0, x) \;=\; 2 + \cos\left(\frac{2\pi x}{L}\right),$$

$$V(t = 0, x) \;=\; -2\;\frac{x-5}{L/2}\left(1 - \left(\frac{|x-5|}{L/2}\right)^{10}\right).$$

This initial velocity is chosen in such a way that, during all the simulation, the rate of shear is in the Zone 3, i.e. in this case $|\partial_x V| \geq 0.22$. In this test, the final time of the simulation is $t = 0.3$.

The fact that, in this regime, the fluid with $\wp = 0.4$ is the less "viscous" can be seen in Figure 5; this fluid has a better ability to move and:

- goes more down near the boundaries ($x \in [0; 1]$ and symmetrically) due to the strong initial velocity that "smashes" the top of the "mountain", ...
- ... induces an expulsion of the fluid to the center, this expulsion creates *(i)* a kind of "splash ring" around $x = 2$ (and symmetrically around $x = 8$) which goes higher for $\wp = 0.4$, ...
- ... as well as *(ii)* a global motion in the inner zone leading to an increase of the free surface at the center ($x \in [2; 5]$ and symmetrically). In a neighborhood of $x = 5$, we clearly see that the free surface with $\wp = 0.4$ is higher than the others.

On the contrary, for the Bingham fluid which is, in this regime, the more "viscous" fluid, we see that the motion is a bit less important than the others. For the third fluid which has the medium "viscosity", its free surface is perfectly bounded by the two others.

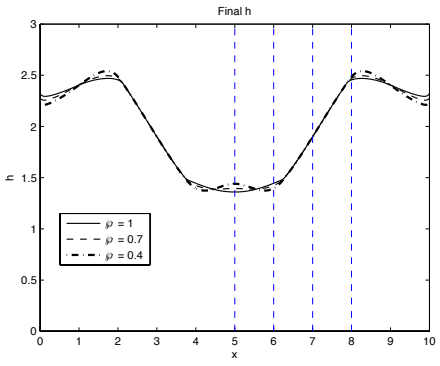

Figure 5: The free surface H at the final time $t = 0.3$, for the three fluids. The dashed vertical lines indicates the probes' locations (denoted as Probe 1, 2, 3 and 4, from left to right respectively).

We add that we performed a mesh refinement study of this test which leads to similar results. This test thus shows the ability of the numerical method to capture the various rheological behaviours of the Herschel-Bulkley model for "high" rates of shear. We will see in the next section that it is also the case for low rate of shear by focusing on the study of the convergence to stationary states of the fluid on an inclined plane ($\theta \neq 0$).

5.3 A case at low rate of shear

In this section, we simulate an academic test of avalanche. This will allow us to show the behaviour of the numerical method with respect to several aspects: *(i)* ability to compute stationary states of a viscoplastic

flow on an inclined plane and *(ii)* role of the Herschel-Bulkley parameter $\wp$ on the evolution of H when the rate of shear is small (in the sense that the flow occurs in Zone 1, described in section 3).

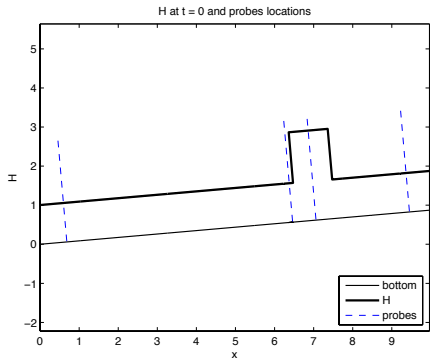

Figure 6: Initial height (thick rectangular pulse), bottom (thin continuous line) and location of the 4 probes (dashed lines) to monitor the evolution of H along time (cf. Figure 8).

To do so, we consider an initial condition such that $\boldsymbol{V}(t=0) \equiv 0$ and

$$H(t=0,x) = \begin{cases} 2.3 & \text{if } 6.5 \leq x \leq 7.5 \\ 1 & \text{otherwise.} \end{cases} \tag{32}$$

This rectangular pulse is above a plane slope inclined with an angle of 5 degrees. As it can be seen on Figure 6, where we also add the location of probe points at $x = 0.6$, 6.4, 7, 9.4. We monitor the evolution of H along time, at these four points.

Physical parameters are those given in section 3. In this context, upon the influence of slope and gravity, the fluid is able to spread and to flow down the slope but there exists a finite time at which the fluid stops, since the load goes below the yield limit.

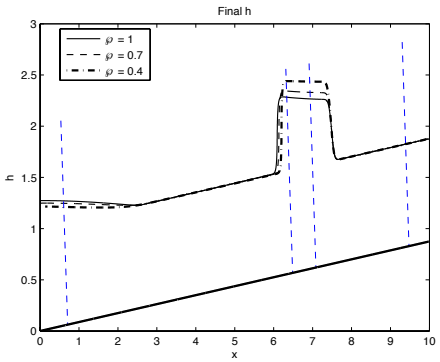

Figure 7: Final heights obtained at the stationary state, for various powers of the Herschel-Bulkley law. Note that, contrary to Figure 6, the scale is not the same between the abscissa and the ordinate.

We perform numerical simulations of the evolution of the free surface and its convergence to a stationary state, for several values of the exponent $\wp$. In particular, we take the Bingham case $\wp = 1$ and two values for a "true" Herschel-Bulkley material, namely $\wp = 0.7$ and $\wp = 0.4$.

The method presented in this paper has been shown to be well-balanced. As a consequence, it is able to compute accurately aforementioned stationary states. To show this, we purposely take a final time of simulation $T = 20$ which is by far greater than the time at which the avalanche stops (approximately 2 for the three fluids considered here).

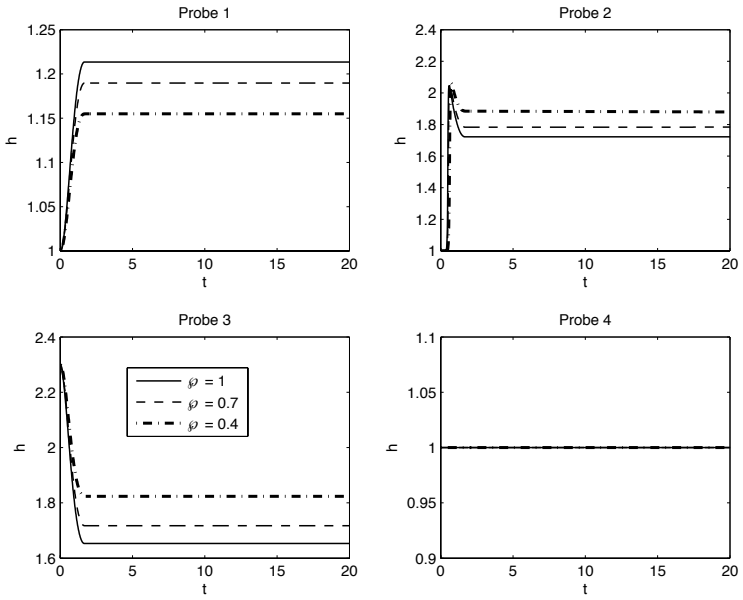

Figure 8: Height for the probe points: $x = 0.6, 6.4, 7, 9.4$.

The stationary heights obtained are shown on Figure 7. The first obvious thing to note, thanks to the graphical help of the probes' location (and comparing Figures 6 and 7), is the motion of the material down the slope: the rectangular pulse is shifted a bit to the left and its height decreases; as a consequence, this flowing material accumulates at the bottom of the slope (see Probe 1), inducing an increase of the height in this zone. The evolution of each height along time, measured at the four probes is shown on Figure 8: we can clearly see that stationary states are obtained since all the curves are flat after $t \approx 2$.

We can also describe the behaviour of the height evolution with respect to the Herschel-Bulkley power. First, it can be noted that the rate of shear in this test is always less than 0.35 and that the flow regime of this test is essentially (i.e. most of the time of the simulation) the one of Zone 1 described in section 3 (rate of shear between 0 and 0.11), especially when the height reaches the stationary state (at $t \approx 2$). The Bingham fluid $\wp = 1$ is thus supposed to flow better than the two others. This can be seen on the final heights, where the Bingham fluid has a hump shape which is below the others (in the neighborhood of $x = 7$) and its level is higher at the bottom of the slope (in the neighborhood of $x = 1$). Furthermore, we see that the position of the three stationary heights is in accordance with the value of $\wp$:

- in the top of the hump, if we denote $h_{\wp_i}$ the height of fluid $\wp_i = \{1, 0.7, 0.4\}$, we have:

$$h_1 \leq h_{0.7} \leq h_{0.4},$$

- whereas, in the bottom of the slope, we have:

$$h_1 \geq h_{0.7} \geq h_{0.4},$$

which is in accordance to the fact that in this regime where the stationary states are reached, the rates of shear are close to zero, leading to an increasing "fluency" of the flow when $\wp$ goes from 0 to 1.

Again, we add that we performed a mesh refinement study of this test which leads to similar results, showing the robustness of the present numerical method.

6 Conclusion

In this work, we present an integrated Herschel-Bulkley model coming from the full 3D Navier-Stokes Herschel-Bulkley equations with a free surface. An asymptotic expansion leads to a viscous shallow water-type model involving a variational inequality.
We then show a coupled augmented Lagrangian / finite volume scheme which fully takes into account both the threshold of plasticity and the power law. The overall method is well balanced, in the sense that it exactly preserves two types of stationary solutions. All these characteristics lead to a scheme which is able to compute the evolution to stationary solutions which can arise in these types of flow (thanks to plastic behaviour). The well balanced property is obtained by remarking that the spatial discretization of all the terms involved must induce a coupling between the height and the speed problem. The overall scheme is exact for the two particular cases mentioned in Proposition 4.
Aforementioned properties are finally illustrated numerically. Thanks to the first numerical test associated to the duct case, for which we have an analytical solution, we show that the implemented scheme is of order 2 in space for a nontrivial stationary solution. The second numerical test is designed to compute a flow at high rate of shear, where the Bingham fluid ($\wp = 1$) is "more viscous" than "true" Herschel-Bulkley fluids ($\wp < 1$). This allows to show the ability of the method to catch the various rheological behaviours of Herschel-Bulkley. As a matter of fact, the third numerical test – an academic test of avalanche – explores small rate of shear where the Bingham fluid is the "less viscous". In both cases, the numerical results are in accordance with the expected physical evolution. Furthermore, the third test is the typical illustration of the well-balanced property of our scheme, since accurate numerical stationary solutions are exhibited for a long time after the reach of the arrested state of the avalanche.

Acknowledgements. The authors would like to thank Didier Bresch for initiating this collaborative work, as well as for his involvement and support. C. A.-R. is supported by French ANR Grant ANR-08-BLAN-0301-01. This research has been partially supported by the Spanish Government Research project MTM2009-07719. Part of this work was done while P. V. was visiting E.D. F.-N. and G. N.-R., from November to December 2010, thanks to a grant from the *Instituto Universitario de Investigación de Matemáticas de la Universidad de Sevilla* (IMUS). P. V. wishes to thank everyone at IMUS for their hospitality. The support of French ANR Grant ANR-08-JCJC-0104-01 is also gratefully acknowledged.

References

[1] C. Acary-Robert, E. Fernández-Nieto, G. Narbona-Reina, and P. Vigneaux. A well-balanced finite volume-augmented Lagrangian method for an integrated Herschel-Bulkley model. *Journal of Scientific Computing*, pages 1–34. http://dx.doi.org/10.1007/s10915-012-9591-x.

[2] C. Ancey and S. Cochard. The dam-break problem for Herschel-Bulkley viscoplastic fluids down steep flumes. *J. Non-Newtonian Fluid Mech.*, 158(1-3):18 – 35, 2009.

[3] N. J. Balmforth, R. V. Craster, A. C. Rust, and R. Sassi. Viscoplastic flow over an inclined surface. *J. Non-Newtonian Fluid Mech.*, 139:103–127, 2006.

[4] E. C. Bingham. *Fluidity and plasticity.* Mc Graw-Hill, 1922.

[5] D. Bresch, E. D. Fernandez-Nieto, I. R. Ionescu, and P. Vigneaux. Augmented Lagrangian method and compressible visco-plastic flows: Applications to shallow dense avalanches. In G. P. Galdi et al., editor, *New Directions in Mathematical Fluid Mechanics*, Advances in Mathematical Fluid Mechanics, pages 57–89. Birkhauser Basel, 2010. http://dx.doi.org/10.1007/978-3-0346-0152-8.

[6] T. Chacón, M. J. Castro, E. D. Fernández-Nieto, and C. Parés. On well-balanced finite volume methods

for non-conservative non-homogeneous hyperbolic systems. *SIAM J. Sci. Comput.*, 29(3):1093–1126, 2007.

[7] E. J. Dean, R. Glowinski, and G. Guidoboni. On the numerical simulation of Bingham visco-plastic flow: old and new results. *J. Non-Newtonian Fluid Mech.*, 142:36–62, 2007.

[8] G. Duvaut and J.-L. Lions. *Inequalities in mechanics and physics*. Springer-Verlag, 1976.

[9] R. Glowinski and P. Le Tallec. *Augmented Lagrangian and operator-splitting methods in nonlinear mechanics*, volume 9 of *SIAM Studies in Applied Mathematics*. Society for Industrial and Applied Mathematics (SIAM), 1989.

[10] I. P. Grinchik and A. Kh. Kim. Axial flow of a nonlinear viscoplastic fluid through cylindrical pipes. *J. Eng. Phys. Thermophys.*, 23:1039–1041, 1972.

[11] W. H. Herschel and T. Bulkley. Measurement of consistency as applied to rubber-benzene solutions. *Am. Soc. Test Proc.*, 26(2):621–633, 1926.